Materials and Design 197 (2021) 109226

Contents lists available at ScienceDirect

Materials and Design

journal homepage: www.elsevier.com/locate/matdes

Cross-scale analysis of nickel Superalloy fatigue using Markov state model-molecular dynamics method

Jianfeng Huang [a,b,*], Don McGlinchey [b], Yi Chen [c,*], Daniel McMahon [a]

[a] Advanced Forming Research Centre, University of Strathclyde, Glasgow PA4 9LJ, United Kingdom
[b] School of Engineering and Built Environment, Glasgow Caledonian University, Glasgow, United Kingdom, G4 0BA
[c] School of Engineering, Newcastle University, Newcastle upon Tyne NE1 7RU, United Kingdom

HIGHLIGHTS

- A novel energy criterion applied for Markov State Model application on crystalline structure investigation.
- A systematic integration of Markov State Mode - Molecular Dynamics methods for time scale bridging.
- Comprehensive microstructure evolution associated with dislocation model.

GRAPHICAL ABSTRACT

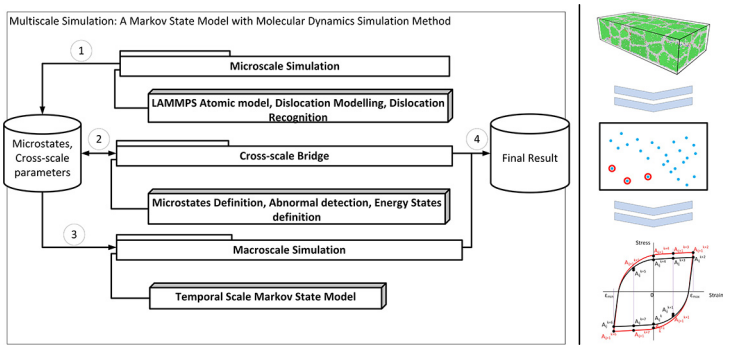

ARTICLE INFO

Article history:
Received 5 March 2020
Received in revised form 28 August 2020
Accepted 9 October 2020
Available online 14 October 2020

Keywords:
Markov state model
Fatigue
Molecular dynamics
Modelling
Multiscale simulation

ABSTRACT

Molecular dynamics (MD) simulation is an advanced method in microscale modelling of material but it depends on the complexity of the model. The performance of MD simulation is poor once the model size is huge. To accelerate the computing of MD simulation, the Markov state model (MSM) can be applied because of the ability to predict a future state of a stochastic system. With the advantage of MSM and MD applied in material modelling, a good result could be expected where the time scale limitation of MD simulation is bridged by MSM method. In this research, an MSM method based on the MD microstates in which a nickel superalloy's atomic model arrangements and their microstructure evolution have been treated with the Markov properties is presented. This MSM is based and classified by a dislocation model which is a fundamental of the microstructural tessellation evolution. The results indicate that the microstructure evolution in a situation of energy minimisation favours the formation of new faults alongside existing ones. And dislocation accumulation on the grain boundary was observed during fatigue resolving. Some dislocations formatted and grown in the middle of coarse grain and penetrated through the grain.

1. Introduction

Numerical simulation methods such as the finite element method [1], boundary element method [2], finite difference method [3], meshfree method [4], discrete dislocation dynamics [5] and MD simulation [6], have become powerful tools for material modelling and engineering simulation at different scales. From the mathematics point of view, the multiscale modelling is the operation of averaging or homogenisation of a system which can be depicted as partial differential equations(PDE), stochastic differential equations(SDE) or ordinary differential equations(ODE) from the macroscale $T(X)$ to microscale $t(x)$ both temporarily and spatially, where $T = t/\varepsilon$, $X = x/\varepsilon$ and ε is a tiny

* Corresponding author.
E-mail addresses: jianfeng.huang@strath.ac.uk (J. Huang), leo.chen@newcastle.ac.uk (Y. Chen).

https://doi.org/10.1016/j.matdes.2020.109226

positive real number. Determining how to establish an effective multiscale correlation analysis method to solve the problem from macroscale to microscale is worth exploring. If there is no macroscale modelling to provide boundary conditions for the interface of microscale modelling, the internal multiscale description will not be clearly stated; if the physical quantity calculated by the microscale method cannot be transmitted to macroscale through a certain equivalent method, the overall physical of the system mechanical properties will not be accurately understood. Therefore, it is necessary to establish an interaction theory and multiscale progressive analysis methods to achieve effective correlation between different scales [7].

At present, the main multiscale numerical simulation methods for solving the cross-scale problems are the multiscale continuous medium method, continuous medium-molecular dynamics coupling method and quasi-continuous medium method. The multiscale method based on the continuous medium was developed to leverage the requirement of homogenisation on the overall domain with macroscale calculation, parameters on different scales correlation and the fine solution on the microscale for local densification [8]. These multiscale methods all are focusing on bridging of the spatial scale of the model. Such combining with FEM and MD or the concurrent quasicontinuum (QC) method can provide a better solution in the properties refinement of the model, especially at some important area in the model where stress concentration is introduced by geometry and structure. But the temporal scale in the fatigue model is relatively long in the real world, especially for the low cycle fatigue problem. The traditional MD model has the advantage in the research of the detail microstructure evolution via the atom trajectory. However, the timescale of an MD simulation is limited to the nano-second if the model is relatively larger in size. The MD model lacks the ability to solve the problem at a long duration time scale. So that other stochastic process methods in probability theory may provide a better solution when applying molecular dynamics. The Markov chain which developed into the Markov state model can predict the model state and material properties by integrating MD simulation [9]. For example, MSM has been successfully applied in biological molecular dynamics simulation to simulate protein folding [10], DNA [11] and ligand-receptor interaction [12]. Also, Sarich [13] had used the concept of MSM discretisation to solve MD optimal control problems in which one computes the optimal external force that drives the molecular system to show an optimised behaviour under certain constraints. It overcomes the limitation of MD simulation in which it is infeasible to compute the rare event statistics directly.

MSM is a robust framework for dynamic system simulation in which the timescale could be extended as it depends only on the probability distribution over the microstates. Many successful examples of applying MSM have already been reported in the field of protein and RNA folding, protein-ligand binding mechanisms and the release of enzymatic reaction's sub-products. The scheme of MSM simulation includes the following stages:

1. Initial the data set;
2. Build up N microstates;
3. Find out the probability matrix between the N microstates transition;
4. Microstates evolution based on Markov Chain;
5. Validation;

One needs to pay attention to MSM stages building when applying this scheme to MD simulation. The first stage is that of selecting a proper MSM method. MSM can predict the events which are characterised as continuous-time and discrete-time. Continuous-time events such as the random walk or protein folding can be simulated by the continuous Markov chain. The microstates which are defined in all the MSM methods, include continuous-time MSM and discrete-time MSM, are discrete. And all of these states chains have the Markov properties that the occurring probability of next states is only related to the previous state. The difference is that the continuous-time MSM is a Markov process with discrete state space but in a continuous-time range. While the discrete-time MSM is a Markov process but with a discrete-time range. Secondly, the microstates of the MSM should be deliberately prepared and clustered before the chain process start. For the microstates generated by MD simulation, the microstate building techniques include kinetic information but begin with a traditional clustering method such as k-means or k-centres using a structural metric [14]. Without such kinetic connecting between each microstate, the basis for the probability matrix in the following stages is difficult to establish [15]. Finally, the MSM microstates transition probability should be defined between each microstate. It is important to eliminate the discreteness effects and shot noise which could lead to noise in the transition probabilities [15]. This noise in the transition matrix will be magnified with the time evolution during MSM processing because the matrix multiplication operation [16]. The Bayesian techniques [17] including the well-chosen prior probabilities is a better solution for this error.

Based on these techniques, the following researches had been done on biomolecular simulation. Thayer et al. [18] employed MSM with MD simulation on ligand binding and allosteric effects in protein folding. They obtained the protein-ligand binding and allostery states and rates from all-atom MD simulation. The all-atom MD simulation is carried out for all the different protein, ligand binding simulation on different constructions. An interesting thing in this MSM method was that the links were defined from the Chapman-Kolmogorov compliant frequency of direct transitions between nodes [18]. The Chapman-Kolmogorov equation is an identity relating the joint probability distributions of different sets of coordinates on a stochastic process [19]. Rosta et al. [20] researched the unbiased MSM application on free energies for dynamics weighted histogram analysis. The weighted histogram analysis method (WHAM) is widely used to obtain accurate free energies from biased molecular simulations. Rosta et al. developed the dynamic histogram analysis method (DHAM) which used a global MSM to obtain the free energy along the reaction coordinate of the MD model. In this MSM application, the transition matrix is constructed by the traditional counting method but with an unbiasing of the transition from multiple umbrella-sampling simulations in the histogram along with discrete reaction coordinates. It found that this DHAM gave accurate free energies even in cases where WHAM fails in terms of the MSM vantage. In the time scale bridging, Voelz et al. [21] predicted the folding of the protein from nanoseconds to microseconds in MD simulations with fidelity to experimental kinetics. The notable contribution of this work is to predict protein folding in a million pathways and extend the simulation time of nanoseconds at the atomic scale to a microsecond. The difficulty of protein folding MSM simulation is the numerous microstates cause the transition probability matrix to be extremely large. This difficulty was overcome by a 'lumping' technique which reduces a total 100,000 microstates into 2000 macrostates. The MSM indicates multiple possible folding pathways can generate different metastable states.

All these studies demonstrated good agreement with available experimental observations which indicates the successful application of MSM scheme with MD simulation. There is no published report on MSM simulation with metal fatigue atomic model, however, these successes and the current situation encourage our research interesting on the nickel-based superalloy fatigue simulation with MSM bridging. This paper has the following structure: Section 2 introduces the MSM method. Section 3 illustrates the detail of the process of MSM-MD simulation in crystalline atomic models. And Section 4 will give the analysis and discussion of the simulation result from the dislocation microstructure evolution to the macroscale fatigue response. Finally, Section 5 gives the conclusion of MSM-MD simulation and future work.

2. MSM-MD modelling

The classic Markov Chain (MC) model is a statistical model which can be used to predict a future event in the discrete-valued Markov process space. Markov Chains are named after Prof. Andrei A. Markov who

was a professor at the University of St. Peterburg and a member of the Russian Academy of Sciences [9]. When talking about Markov Chain, it always begins with the Markov property. In probability theory, the Markov property is a probability property of a statistics process whose probability of future state depends only upon the present state [16]. One can be called a Markov process if a stochastic process has such property. Generally, a Markov Chain is a type of Markov process that has either discrete state-space or discrete index set. The traditional Markov Chains theory is discrete-time Markov chains. Based on the traditional MC and due to the demands of various applications, different types of Markov Chain models are illustrated and developed by researchers. Those alternative Markov Chains include continuous-time MC, hidden MC, and high order MC which is from the discrete-time MC [16].

MC is widely applied in various domains [22] because of the general and simple properties with good probability result. The thermodynamic and statistic mechanics problems in physics, enzyme folding and action in chemistry, data compression and pattern recognition in information technology, market prediction in economics and finance, protein folding and unfolding in biology and even in games. The application of Markov Chain in data compression is named Dynamic Markov Compression (DMC) which has a good compression ratio and moderate compression speed [23]. In bio-molecular dynamics, the application of Markov Chain to fill the gap between the simulation result in nanoscope and the experiment results in macroscope is widely researched. In these applications, the metastable protein states with special transition pathways and transition probabilities matrix have been investigated for the key characteristic of MSM for biological molecular study. Usually, these metastable states are related to the system potential energy which will remain in the vicinity of the main wells for a long time before making a transition to another well. After the protein molecular trajectories are assigned to each microstate, the probability of microstates transition can be calculated by counting their transition times between each state. Finally, with the transition matrix, one can predict future events or microstates which would happen for a special time lag or period. This inspired the methodology used in this work in material molecular dynamics simulation which only lasts for several nanoseconds, and lacks comparability with experimental results. The MSM method was expected to solve this problem.

The classic MC is modelled to predict the stochastic process in which a state is only related to the previous one. In other words, the probability of the event occurring in the current state is only decided by the event just before it. To begin with this model, it needs to define the state in this stochastic process as A_n, $n = 0,1,2, \ldots$ that take a finite set. Based on the assumption of Markov properties, the transition probability P_{ij} can be defined and represent the probability that the process will take a transition to the state i if the process is in current state j. By applying the ergodic visiting algorithm on all states between each other, a transition probability matrix by which the Markov process is predicted could be given.

$$\boldsymbol{P} = \begin{bmatrix} P_{01} & P_{02} & \cdots & P_{0n} \\ P_{11} & P_{12} & \cdots & P_{1n} \\ \vdots & \ddots & \cdots & \vdots \\ P_{n1} & P_{n2} & \cdots & P_{nn} \end{bmatrix} \tag{1}$$

For the states in nth step, the probability of each state would have occurred can be defined as:

$$A^{(n)} = \left(A_1^{(n)}, A_2^{(n)}, \ldots\right) \mid \sum A_i^{(n)} = 1 \tag{2}$$

And for the next time step with the lag time τ, the probability for each state is:

$$A^{(n+1)} = \boldsymbol{P} A^{(n)} \tag{3}$$

Given the state in the very beginning of this stochastic process, one can predict the future state transition with the probability matrix by Eq. 3. Finally, it turns into the form in Eq. 4.

$$A^{(n+1)} = \boldsymbol{P}^n A^{(0)} \tag{4}$$

For the fully reversed fatigue load process as illustrated in Fig. 1, in a load cycle, the stress-strain state can be divided into a different instantaneous state by the equivalent strain interval. For example, in a load cycle of Fig. 1, the instantaneous state can be defined as A_{ij}^k, where index k represents the different strain load state as depicted in Table 1. Moreover, indices i, j denote the different irreversible state and cycle respectively. After the instantaneous state defined, each state can be simulated in LAMMPS for MD simulation to get the instantaneous stress, energy, and other physical properties. However, the consecutive bridge between two neighbour states can be simulated with the actual strain load in another simulation. Once the states are defined, an initialised states space can be defined by a fixed number of cycles represented by the index j, for example, $j = 6$ for six cycles of the load. According to the same strain state, once these initial states are decided, the probability of transition from previous strain state to the following next strain state between different cycle can be considered.

For all states in strain state k, it can be considered to be a collection of all atoms' coordinates - that is $C_j^k(\boldsymbol{p_0}, \boldsymbol{p_1}, \ldots, \boldsymbol{p_n}, \boldsymbol{q_0}, \boldsymbol{q_1}, \ldots, \boldsymbol{q_n})(j = 1, \ldots, J)$. For any state with index k to another state $k + 1$, this transition assumed to be a stochastic process because the interval time between two states is long enough compared to the instantaneous simulation time, and the atom coordinates could be stochastic with the long time interval. The counting method is used in the traditional MSM method to determine the transition probability between the two states. In this method, the transition times for all events have been counted at first, and then, the probability is the transition times between special two states divided by the total transition times. However, in this model, the probability can be determined by the system energy gap between different state.

For each microstate, the system energy for state i, j, k is E_{ij}^k, the energy gap between two different strain state k and $k + 1$ is $E_{ij}^k - E_{ij}^{k+1}$. According to the energy dissipation as observed in paper [24], the energy gap is a better criterion for the probability determination.

If in a reversible process where the index i is the same, and then with the determination of the transition probability, the probability matrix of these transitions is $\boldsymbol{P}$. As shown in Table 2, the value 0 means there is no change from one state to another. Otherwise, it evaluates the probability of transition from state A to another state A' is p.

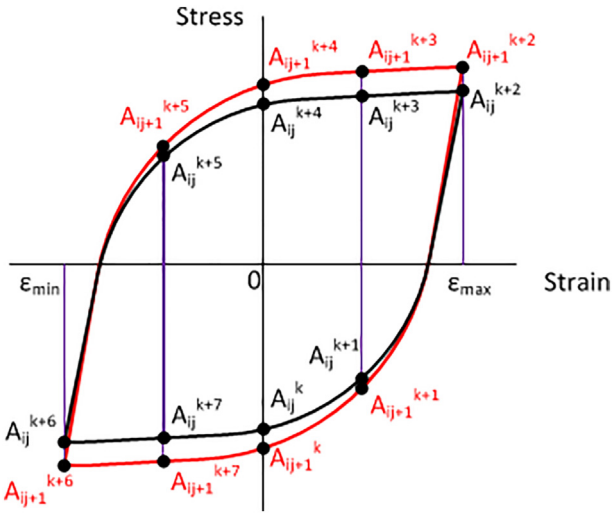

Fig. 1. The fatigue process illustrated as stress strain curve.

Table 1
The representation of indices of *i, j, k*.

Index	1	2	3	4	5	6	7	8
i	Irreversible state 1–8							
j	cycle 1	cycle 2	cycle 3	cycle 4	cycle 5	cycle 6	cycle 7	cycle 8
k	Strain 0 load	Strain $0.5\varepsilon_{max}$ load	Strain ε_{max} load	Strain $0.5\varepsilon_{max}$ unload	Strain 0 unload	Strain $0.5\varepsilon_{min}$ unload	Strain ε_{min} unload	Strain $0.5\varepsilon_{min}$ load

Table 2
Probability matrix of transitions between different strain states within a reversible process.

	A_{11}^1	A_{11}^2	A_{11}^3	A_{11}^4	A_{12}^1	A_{12}^2	A_{12}^3	A_{12}^4
A_{11}^1	0	0	0	p_{14-21}	0	0	0	p
A_{11}^2	p_{11-12}	0	0	0	p_{21-12}	0	0	0
A_{11}^3	0	p_{12-13}	0	0	0	p_{22-13}	0	0
A_{11}^4	0	0	p_{13-14}	0	0	0	p_{23-14}	0
A_{12}^1	0	0	0	p_{14-21}	0	0	0	p_{24-11}
A_{12}^2	p_{11-22}	0	0	0	p_{21-22}	0	0	0
A_{12}^3	0	p_{12-23}	0	0	0	p_{22-23}	0	0
A_{12}^4	0	0	p_{13-24}	0	0	0	p_{23-24}	0

Since the plastic deformation in the material is irreversible, some normal states evidently are not reachable after the plastic deformation appears. Thus, the probability of transition from plastic deformation state to the previous normal state is zero. Therefore, the new transform probability matrix of the irreversible process is in Table 3

$$\boldsymbol{S_n} = \boldsymbol{P}^n \cdot \boldsymbol{S_1} \tag{5}$$

Given a initial state vector, $\boldsymbol{S_1} = (S_{11}^1, S_{11}^2 \ldots, S_{ij}^k) = (1,0,\ldots,0)$, where 1 denotes this A_{11}^1 state is present. The nth state $\boldsymbol{S_n}$ can be predicted by the Eq. 5.

. Simulations

By implementing the MSM-MD described in Section 2, the microstates of MD models are initialised with the EAM potential proposed by Mishin [25]. But the simulation box is limited in a small size due to performance reasons. This box is set to 200 Å ×100Å ×20Å in the x y and z directions separately. The time interval for each microstates is set according to the checkpoints numbers for each cycle. For example, if the number of checkpoints in one cycle is 8, the time interval between each microstate is $\frac{1}{8}T$ where T is a fatigue cycle time. The initialisation number of the microstate of the MSM model can be set to 48. In this MD simulation, the deformation strain is set to 0.5 % ,1.0% and 1.5% separately. Also, the models are divided into two regions in the centre. In the left half side is FCC γ phase and in the right half side is the FCC γ′ phase. In each region, to research the effect of the polycrystalline superalloys, a $3 \times 3 \times 1$ Voronoi tessellation [26] was build up. In this model, to illustrate the effect of crack, two small regions near the upper boundary of the simulation box were created, and the bond relation of the atoms in the two regions was eliminated for a crack. The system temperature was elevated to 900K and relaxed by getting the steady state at the beginning. In each state, to evaluate the physical properties of the model, 20000 simulation steps were performed with an initialised speed for each atom. The atom coordinates, stress and other information stored onto a disk. After this simulation, the model would be elongated to the next state with the accurate deformation rate due to the total deformation strain amplitude and the number of states in a cycle. The central atom information and virial stress of atom were statistically calculated for each 2000 steps. After all initialised state simulated, dislocation energy of each state was calculated.

The test designed the parameter of the strain rate and the size of the margin box size various from 5 to 25 by step of 5 and the position of the box from 15 to 25 in Y directions.

Table 3
Probability matrix of transitions in different irreversible states.

	A_1	A_2	A_3	A_4
A_1	0	0	0	0
A_2	p_{1-2}	0	0	0
A_3	0	p_{2-3}	0	0
A_4	0	0	p_{3-4}	0

. Microstate definition

The essentials of the MSM, by recalling the notion in Section 2, are the proper partitioning of the conformational space which the metastable states correspond to distinctive energy minima and the transfer probability matrix(TPM) which is the determinant of MSM result. According to [10], this partitioning can be accomplished by two steps, microstate clustering and the macrostate lumping. While in this research, according to the difference of dislocation conformation against the biological protein folding conformation, the microstate clustering and macrostate lumping method is not suitable. However, the energy minima and the kinetic behaviour similarity can be adopted. The microstate definition is achieved by the following stages, 1) Dislocation recognition which is defined in [27] and 2) Dislocation energy minimisation classification. The first stage of dislocation recognition is similar to the microstate clustering which determines the MD particles trajectories into a different conformation. The similarity of the dislocation structure and kinetic characteristic could be measured by the geometry quantities of the dislocation.

The maximum microstates number depends on the theoretical requirement of MSM and the actual computation. From MSM side, less initial microstates given, more performance gained. However, to simulate the reality, it will lose important information of the fatigue process. While from the computational capacity side, the number of maximum microstates lies on the model size very much. If the size is too big, for example, more than half million atoms, it will be very expensive to get the simulation finish. If the number of microstates too much during MSM simulation, at first, it will cause the performance issue because of the increased transaction between each microstate. Also, the computation of the probability matrix will be exponentially growth during MSM prediction process. Thus, it could slow down the computing. On the other hand, more initial microstates would lead to a precise MSM prediction result with a fine hysteresis loop curve.

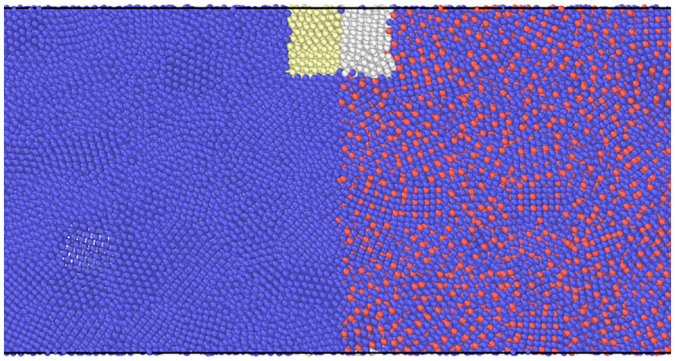

Fig. 2. The Initialization Configuration of MD Model. γ phase is designed in the left side with all blue atoms while γ′ phase in the right side with blue and red atoms. The yellow and white atoms indicate the two area which atom interaction is eliminated as designed. (For interpretation of the references to colour in this figure legend, the reader is referred to the web version of this article.)

In this simulation, the MD model definition is in Fig. 2, for each stage, a serial of dislocation configuration as an example is generated by the MD simulation and dislocation recognition methodology as shown in Fig. 4. The dislocation energy was measured by the modified MD simulation and an example of the energy configuration is displayed in Fig. 3. The dislocation energy is a result of the energy summation of dislocation atoms calculated by modified LAMMPS.

. The probability of microstate transformation

After the microstate is defined clearly, the probability can be defined in Table 2 as shown in Section 2. To find the probability of the state transfer between different energy states, the reciprocal of energy difference is required for an energy difference minimization. The total energy difference is defined as:

$$M = \sum_i \frac{1}{E_{ij}^k - E_{ij}^{k+1}} \tag{6}$$

And then the probability of the state transfer from state $i(j_1)k$ to state $ij_2(k+1)$ is the proportion of current reciprocal of the energy difference over the total reciprocal of the energy difference.

$$P_j = \frac{\frac{1}{E_{ij_1}^k - E_{ij_2}^{k+1}}}{M} = \frac{\frac{1}{E_{ij}^k - E_{ij}^{k+1}}}{\sum_i \frac{1}{E_{ij}^k - E_{ij}^{k+1}}} \tag{7}$$

As shown in the designation of MSM microstates, a total of 48 microstates divided the fatigue cycles evenly. The number of microstates affects the precision of the simulation result and the simulation performance. If this number is small, the lag time between each microstate will increase and the simulation result would be too fuzzy to reveal the truth. While on the contrary, the simulation performance would be extremely poor in both MD simulation and MSM simulation. In this simulation, each state has corresponding strain states in the fatigue test. The probability matrix is demonstrated in Table 4. This matrix is a sparse matrix according to the feature of the microstates definition and their conversion between each other. Thus, this speciality of the transfer probability matrix could reduce computing storage during the MSM simulation.

. State evolution

The microstate of MSM usually clusters into macrostate in traditional MSM model in biology molecular dynamics simulation [15]. This clustering of the microstates is according to the kinetic and structural similarity of the atomic arrangement. However, in this fatigue simulation, the external condition of strain state is an additional one because of the microstructure evolution of the system structure is followed not only in time but also the strain state. The microstate evolution according to the MSM prediction is given by the systematic methodology.

First, the initial state of the fatigue process could be represented by a vector with the length of the total initial microstates. The index of elements in this vector represents each microstate, and the element in this index represents the occurrence of the event (0 means the non-presence of the microstate or 1 means the presence of the microstate). For example, for the initial state, the known state is the first microstates. Thus, the first element of this vector is 1. According to the exclusivity of the microstates, the value of other sites must be 0. So the vector is:

$$A1 = \left(1 \underbrace{0\ 0\ \ldots\ 0}_{N-1}\right)^T \tag{8}$$

where the N is the number of total microstates.

Second, according to MSM, the prediction of the future event in the nth time interval could be the result of the product of the initial state vector and the nth power of the transfer probability matrix in Eq. 5. After this operation, the result is another vector with the probabilities

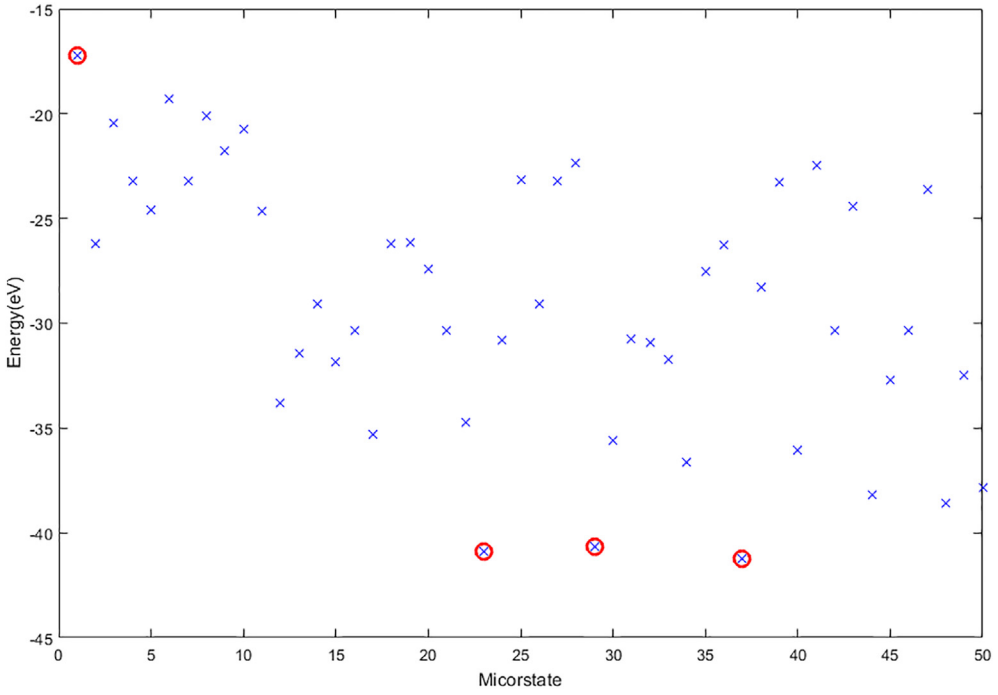

Fig. 3. Anomaly state detection according to the microstate's dislocation energy states data classification.

Table 4
The probability matrix of one example with 48 initiation microstates.

	A1	A2	A3	A4	A5	A6	A7	A8	A9	A10	A11	A12	A13	A14	A15	A16	A17	A18	A19	A20	A21	A22	A23
A1	0	0	0	0	0	0	0	0.086	0	0	0	0	0	0	0	0.0433	0	0	0	0	0	0	0
A2	0.3097	0	0	0	0	0	0	0	0.2073	0	0	0	0	0	0	0	0.0841	0	0	0	0	0	0
A3	0	0.1412	0	0	0	0	0	0	0	0.1498	0	0	0	0	0	0	0	0.3947	0	0	0	0	0
A4	0	0	0.2013	0	0	0	0	0	0	0	0.7110	0	0	0	0	0	0	0	0.1000	0	0	0	0
A5	0	0	0	0.1198	0	0	0	0	0	0	0	0.1263	0	0	0	0	0	0	0	0.1518	0	0	0
A6	0	0	0	0	0.1962	0	0	0	0	0	0	0	0.5897	0	0	0	0	0	0	0	0.7499	0	0
A7	0	0	0	0	0	0.0128	0	0	0	0	0	0	0	0.0676	0	0	0	0	0	0	0	0.0639	0
A8	0	0	0	0	0	0	0.0770	0	0	0	0	0	0	0	0.0105	0	0	0	0	0	0	0	0.0722
A9	0	0	0	0	0	0	0	0.1432	0	0	0	0	0	0	0	0.3769	0	0	0	0	0	0	0
A10	0.3699	0	0	0	0	0	0	0	0.1787	0	0	0	0	0	0	0	0.0791	0	0	0	0	0	0
A11	0	0.3525	0	0	0	0	0	0	0	0.3439	0	0	0	0	0	0	0	0.2449	0	0	0	0	0
A12	0	0	0.0805	0	0	0	0	0	0	0	0.0047	0	0	0	0	0	0	0	0.5185	0	0	0	0
A13	0	0	0	0.1486	0	0	0	0	0	0	0	0.1590	0	0	0	0	0	0	0	0.0781	0	0	0
A14	0	0	0	0	0.3041	0	0	0	0	0	0	0	0.1348	0	0	0	0	0	0	0	0.0632	0	0
A15	0	0	0	0	0	0.8600	0	0	0	0	0	0	0	0.1839	0	0	0	0	0	0	0	0.1820	0
A16	0	0	0	0	0	0	0.2371	0	0	0	0	0	0	0	0.0645	0	0	0	0	0	0	0	0.2443
A17	0	0	0	0	0	0	0	0.2882	0	0	0	0	0	0	0	0.0759	0	0	0	0	0	0	0
A18	0.1021	0	0	0	0	0	0	0	0.2068	0	0	0	0	0	0	0	0.4000	0	0	0	0	0	0
A19	0	0.0646	0	0	0	0	0	0	0	0.0707	0	0	0	0	0	0	0	0.0639	0	0	0	0	0
A20	0	0	0.1715	0	0	0	0	0	0	0	0.0823	0	0	0	0	0	0	0	0.0944	0	0	0	0
A21	0	0	0	0.1201	0	0	0	0	0	0	0	0.1635	0	0	0	0	0	0	0	0.0673	0	0	0
A22	0	0	0	0	0.2989	0	0	0	0	0	0	0	0.1403	0	0	0	0	0	0	0	0.0650	0	0
A23	0	0	0	0	0	0.0141	0	0	0	0	0	0	0	0.0783	0	0	0	0	0	0	0	0.0738	0
A24	0	0	0	0	0	0	0.2156	0	0	0	0	0	0	0	0.0981	0	0	0	0	0	0	0	0.2193
A25	0	0	0	0	0	0	0	0.1032	0	0	0	0	0	0	0	0.0138	0	0	0	0	0	0	0
A26	0.1139	0	0	0	0	0	0	0	0.2996	0	0	0	0	0	0	0	0.2527	0	0	0	0	0	0
A27	0	0.0663	0	0	0	0	0	0	0	0.0725	0	0	0	0	0	0	0	0.0666	0	0	0	0	0
A28	0	0	0.0333	0	0	0	0	0	0	0	0.0023	0	0	0	0	0	0	0	0.0714	0	0	0	0
A29	0	0	0	0.0406	0	0	0	0	0	0	0	0.2295	0	0	0	0	0	0	0	0.0279	0	0	0
A30	0	0	0	0	0.0148	0	0	0	0	0	0	0	0.0031	0	0	0	0	0	0	0	0.0020	0	0
A31	0	0	0	0	0	0.0207	0	0	0	0	0	0	0	0.1449	0	0	0	0	0	0	0	0.1350	0
A32	0	0	0	0	0	0	0.1009	0	0	0	0	0	0	0	0.0177	0	0	0	0	0	0	0	0.0958
A33	0	0	0	0	0	0	0	0.2045	0	0	0	0	0	0	0	0.1476	0	0	0	0	0	0	0
A34	0.0505	0	0	0	0	0	0	0	0.0512	0	0	0	0	0	0	0	0.0848	0	0	0	0	0	0
A35	0	0.3752	0	0	0	0	0	0	0	0.3629	0	0	0	0	0	0	0	0.2297	0	0	0	0	0
A36	0	0	0.2785	0	0	0	0	0	0	0	0.0636	0	0	0	0	0	0	0	0.1104	0	0	0	0
A37	0	0	0	0.0693	0	0	0	0	0	0	0	0.1832	0	0	0	0	0	0	0	0.0440	0	0	0
A38	0	0	0	0	0.0280	0	0	0	0	0	0	0	0.0064	0	0	0	0	0	0	0	0.0041	0	0
A39	0	0	0	0	0	0.0198	0	0	0	0	0	0	0	0.0526	0	0	0	0	0	0	0	0.0508	0
A40	0	0	0	0	0	0	0.1778	0	0	0	0	0	0	0	0.4401	0	0	0	0	0	0	0	0.1767
A41	0	0	0	0	0	0	0	0.1740	0	0	0	0	0	0	0	0.3423	0	0	0	0	0	0	0
A42	0.0538	0	0	0	0	0	0	0	0.0563	0	0	0	0	0	0	0	0.0993	0	0	0	0	0	0
A43	0	0	0	0	0	0	0	0	0	0	0	0	0	0	0	0	0	0	0	0	0	0	0
A44	0	0	0.2347	0	0	0	0	0	0	0	0.1359	0	0	0	0	0	0	0	0.1051	0	0	0	0
A45	0	0	0	0.5014	0	0	0	0	0	0	0	0.1383	0	0	0	0	0	0	0	0.6307	0	0	0
A46	0	0	0	0	0.1577	0	0	0	0	0	0	0	0.1254	0	0	0	0	0	0	0	0.1156	0	0
A47	0	0	0	0	0	0.0724	0	0	0	0	0	0	0	0.4725	0	0	0	0	0	0	0	0.4943	0
A48	0	0	0	0	0	0	0.1912	0	0	0	0	0	0	0	0.3690	0	0	0	0	0	0	0	0.1916

for each state. For example, in the second step, the result of this step is a vector:

$$A1\beta = \left(1 \underbrace{0\ 0\ \ldots\ 0}_{N-1}\right)^T \tag{9}$$

The value of each element indicates the probability of which of these microstates have the chance to occur in the current state. The bigger the value is, the higher the opportunity this microstate would be present. That is not the final result of the current state that we expected. What we expected is the confirmation of the occurrence of a microstate.

Finally, to determine this with the MSM result, the MC method could be applied. The process is illustrated as the following.

Get the probability result and sort the list from high to low.

Create a series of segment lines which length is the value in the MSM result. A total length would be 1.

In a loop with the iteration number, create a random number between (0 1) with the uniform distribution, and record the index number of the segment which the random number belong to. And add this to appearance of this segment.

After the loop is finished, count the maximum value of the appearance of all segment, get this index as the result.

. MSM result and discussion

The MSM initial state is shown in Table 5. By applying the MSM and MC prediction, the result of the prediction in the first 100 states in a total 1000 prediction for simulation (simulation number index) is displayed in Fig. 5. By re-arrangement these microstates according to the MSM result, the stress-strain response have been collected and displayed in Fig. 6. In this stress-strain response results (Figs. 6 and 7), it indicates the peak stress at the 4th cycle is about 700*MPa*, after a few cycles to 21st cycle, the stress increases to near 800*MPa*, then it drops down to 570*MPa* at 111st cycle. This indicates that material hardening occurs at the first stage and then finally the softening of the material can be observed. However, in this result, the valley stresses during these cycles are at the same level. But the valley stress vibration was observed in another test as shown in Fig. 8. In Fig. 7, this result reflects that the energy differences between these microstates of minimum strain stage and microstates in the previous stage have an outstanding gap than other microstates of minimum strain stages. Such a difference cause the MSM prediction at the same result for a process evolution. But in Fig. 8, the vibration of valley stress indicates the energy differences between the microstates of minimum strain stage have no extreme gaps. So that the MSM predicts the result with the fluctuation of the stress state.

The hysteresis loop in the MD simulation indicates the plastic deformation according to the external loading. Since the MD simulation is

A24	A25	A26	A27	A28	A29	A30	A31	A32	A33	A34	A35	A36	A37	A38	A39	A40	A41	A42	A43	A44	A45	A46	A47	A48
0.0335	0	0	0	0	0	0	0	0.0572	0	0	0	0	0	0	0	0.0265	0	0	0	0	0	0	0	0.0121
0	0.1061	0	0	0	0	0	0	0	0.0296	0	0	0	0	0	0	0	0.0610	0	0	0	0	0	0	0
0	0	0.2424	0	0	0	0	0	0	0	0.0898	0	0	0	0	0	0	0	0.1498	0	0	0	0	0	0
0	0	0	0.1099	0	0	0	0	0	0	0	0.7824	0	0	0	0	0	0	0	0	0	0	0	0	0
0	0	0	0	0.1468	0	0	0	0	0	0	0	0.0562	0	0	0	0	0	0	0	0.1062	0	0	0	0
0	0	0	0	0	0.2434	0	0	0	0	0	0	0	0.2141	0	0	0	0	0	0	0	0.1522	0	0	0
0	0	0	0	0	0	0.1558	0	0	0	0	0	0	0	0.1455	0	0	0	0	0	0	0	0.0659	0	0
0	0	0	0	0	0	0	0.0540	0	0	0	0	0	0	0	0.1045	0	0	0	0	0	0	0	0.0069	0
0.2032	0	0	0	0	0	0	0	0.1121	0	0	0	0	0	0	0	0.1012	0	0	0	0	0	0	0	0.0537
0	0.1041	0	0	0	0	0	0	0	0.0273	0	0	0	0	0	0	0	0.0552	0	0	0	0	0	0	0
0	0	0.3376	0	0	0	0	0	0	0	0.0549	0	0	0	0	0	0	0	0.0858	0	0	0	0	0	0
0	0	0	0.4747	0	0	0	0	0	0	0	0.0038	0	0	0	0	0	0	0	0	0	0	0	0	0
0	0	0	0	0.1646	0	0	0	0	0	0	0	0.4783	0	0	0	0	0	0	0	0.2849	0	0	0	0
0	0	0	0	0	0.1815	0	0	0	0	0	0	0	0.1147	0	0	0	0	0	0	0	0.3669	0	0	0
0	0	0	0	0	0	0.1717	0	0	0	0	0	0	0	0.1758	0	0	0	0	0	0	0	0.3786	0	0
0	0	0	0	0	0	0	0.2803	0	0	0	0	0	0	0	0.0833	0	0	0	0	0	0	0	0.1734	0
0.0695	0	0	0	0	0	0	0	0.4335	0	0	0	0	0	0	0	0.0860	0	0	0	0	0	0	0	0.0326
0	0.1400	0	0	0	0	0	0	0	0.6506	0	0	0	0	0	0	0	0.2038	0	0	0	0	0	0	0
0	0	0.0550	0	0	0	0	0	0	0	0.3480	0	0	0	0	0	0	0	0.3130	0	0	0	0	0	0
0	0	0	0.1035	0	0	0	0	0	0	0	0.0840	0	0	0	0	0	0	0	0	0	0	0	0	0
0	0	0	0	0.1667	0	0	0	0	0	0	0	0.2384	0	0	0	0	0	0	0	0.2050	0	0	0	0
0	0	0	0	0	0.1830	0	0	0	0	0	0	0	0.1164	0	0	0	0	0	0	0	0.3512	0	0	0
0	0	0	0	0	0	0.1573	0	0	0	0	0	0	0	0.1481	0	0	0	0	0	0	0	0.0718	0	0
0	0	0	0	0	0	0	0.2335	0	0	0	0	0	0	0	0.0912	0	0	0	0	0	0	0	0.6697	0
0.0115	0	0	0	0	0	0	0	0.0445	0	0	0	0	0	0	0	0.0108	0	0	0	0	0	0	0	0.0046
0	0.1333	0	0	0	0	0	0	0	0.2538	0	0	0	0	0	0	0	0.6231	0	0	0	0	0	0	0
0	0	0.0571	0	0	0	0	0	0	0	0.4531	0	0	0	0	0	0	0	0.3669	0	0	0	0	0	0
0	0	0	0.0744	0	0	0	0	0	0	0	0.0018	0	0	0	0	0	0	0	0	0	0	0	0	0
0	0	0	0	0.1924	0	0	0	0	0	0	0	0.0389	0	0	0	0	0	0	0	0.0530	0	0	0	0
0	0	0	0	0	0.0226	0	0	0	0	0	0	0	0.0074	0	0	0	0	0	0	0	0.0071	0	0	0
0	0	0	0	0	0	0.1617	0	0	0	0	0	0	0	0.1560	0	0	0	0	0	0	0	0.0972	0	0
0	0	0	0	0	0	0	0.0753	0	0	0	0	0	0	0	0.4984	0	0	0	0	0	0	0	0.0107	0
0.1517	0	0	0	0	0	0	0	0.2008	0	0	0	0	0	0	0	0.3405	0	0	0	0	0	0	0	0.0928
0	0.2720	0	0	0	0	0	0	0	0.0180	0	0	0	0	0	0	0	0.0268	0	0	0	0	0	0	0
0	0	0.3077	0	0	0	0	0	0	0	0.0540	0	0	0	0	0	0	0	0.0843	0	0	0	0	0	0
0	0	0	0.1217	0	0	0	0	0	0	0	0.0448	0	0	0	0	0	0	0	0	0	0	0	0	0
0	0	0	0	0.1755	0	0	0	0	0	0	0	0.0818	0	0	0	0	0	0	0	0.0990	0	0	0	0
0	0	0	0	0	0.0512	0	0	0	0	0	0	0	0.0157	0	0	0	0	0	0	0	0.0140	0	0	0
0	0	0	0	0	0	0.1844	0	0	0	0	0	0	0	0.2044	0	0	0	0	0	0	0	0.1734	0	0
0	0	0	0	0	0	0	0.1676	0	0	0	0	0	0	0	0.1171	0	0	0	0	0	0	0	0.0539	0
0.5305	0	0	0	0	0	0	0	0.1518	0	0	0	0	0	0	0	0.4347	0	0	0	0	0	0	0	0.8041
0	0.2444	0	0	0	0	0	0	0	0.0205	0	0	0	0	0	0	0	0.0299	0	0	0	0	0	0	0
0	0	0	0	0	0	0	0	0	0	0	0	0	0	0	0	0	0	0	0	0	0	0	0	0
0	0	0	0.1157	0	0	0	0	0	0	0	0.0831	0	0	0	0	0	0	0	0	0	0	0	0	0
0	0	0	0	0.1538	0	0	0	0	0	0	0	0.1062	0	0	0	0	0	0	0	0.2518	0	0	0	0
0	0	0	0	0	0.3180	0	0	0	0	0	0	0	0.5314	0	0	0	0	0	0	0	0.1084	0	0	0
0	0	0	0	0	0	0.1689	0	0	0	0	0	0	0	0.1700	0	0	0	0	0	0	0	0.2129	0	0
0	0	0	0	0	0	0	0.1890	0	0	0	0	0	0	0	0.1052	0	0	0	0	0	0	0	0.0852	0

strain-controlled, the total strain amplitude is always in the same value. However, the stress response could change due to the structure rearrangement(Fig. 6). In this result, the absolute values of peak and valley stress responses are increased after a few cycles. Also, by investigating the detail of each cycle, the hysteresis loop could be clearly identified as displayed in Fig. 7. The result of hysteresis loop reveals a peak stress increase after a few cycles in the first stage and then decrease at the end of the test. From this image, it can be seen that the area of the hysteresis loop steadily increases. This indicates material hardening at first and then the softening, while the plastic deformation constantly increases with the energy dissipation.

By comparing the stress-strain response result with other test cases which the broken bond area is increased, it seems the area of the hysteresis loop is proportional with this factor. (Fig. 9). This configuration of the test model aims to simulate the situation of microcrack performed in the material due to the cyclical loading. The microcrack, a broken bond atomic configuration in this simulation, is an essential characteristic of fatigue loading [28]. In this result, the half-life cycle stress-strain responses of these test case with different size (5 Å to 20 Å) of microcrack were plotted in Fig. 9. The increase of the microcrack area, the higher hysteresis loop area are observed. This indicates that the energy dissipation increase is associated with higher plastic deformation.

Also, when the microcrack size increased, the peak and valley stresses of fatigue response in this simulation are also shrunk due to the extended broken bonds of atoms. This is relatively clear from Eq. 10 which is in the formation listed below [29].

$$A1\beta = \left(1 \underbrace{0\ 0\ \ldots\ 0}_{N-1}\right)^{T} \tag{10}$$

where the subscripts i, j denote atom coordinates and α, β indicate the different atom numbers. V denotes the summation of atom volume, m is the mass of the atom, v with the subscripts is the quantity of projection of the specified atom velocity along the indicated direction. The function $\phi(r)$ is the potential energy of the atom. r is the interatomic distance. Similarly, r with the subscript is the projection of the distance vector r along coordinate i or j. In this equation, the first term $m_\alpha v_{\alpha,}$ ${}_i v_{\alpha,j}$ is the kinetic contribution which indicates that the force generated by the motion of atoms across a fixed spatial surface, and the second

Table 5
Markov Chain initial state list in a index sequence with 6 cycles.

Cycles	Strain	0%	0.5%	1%	0.5%	0%	−0.5%	−1%	−0.5%
1		1	2	3	4	5	6	7	8
2		9	10	11	12	13	14	15	16
3		17	18	19	20	21	22	23	24
4		25	26	27	28	29	30	31	32
5		33	34	35	36	37	38	39	40
6		41	42	43	44	45	46	47	48

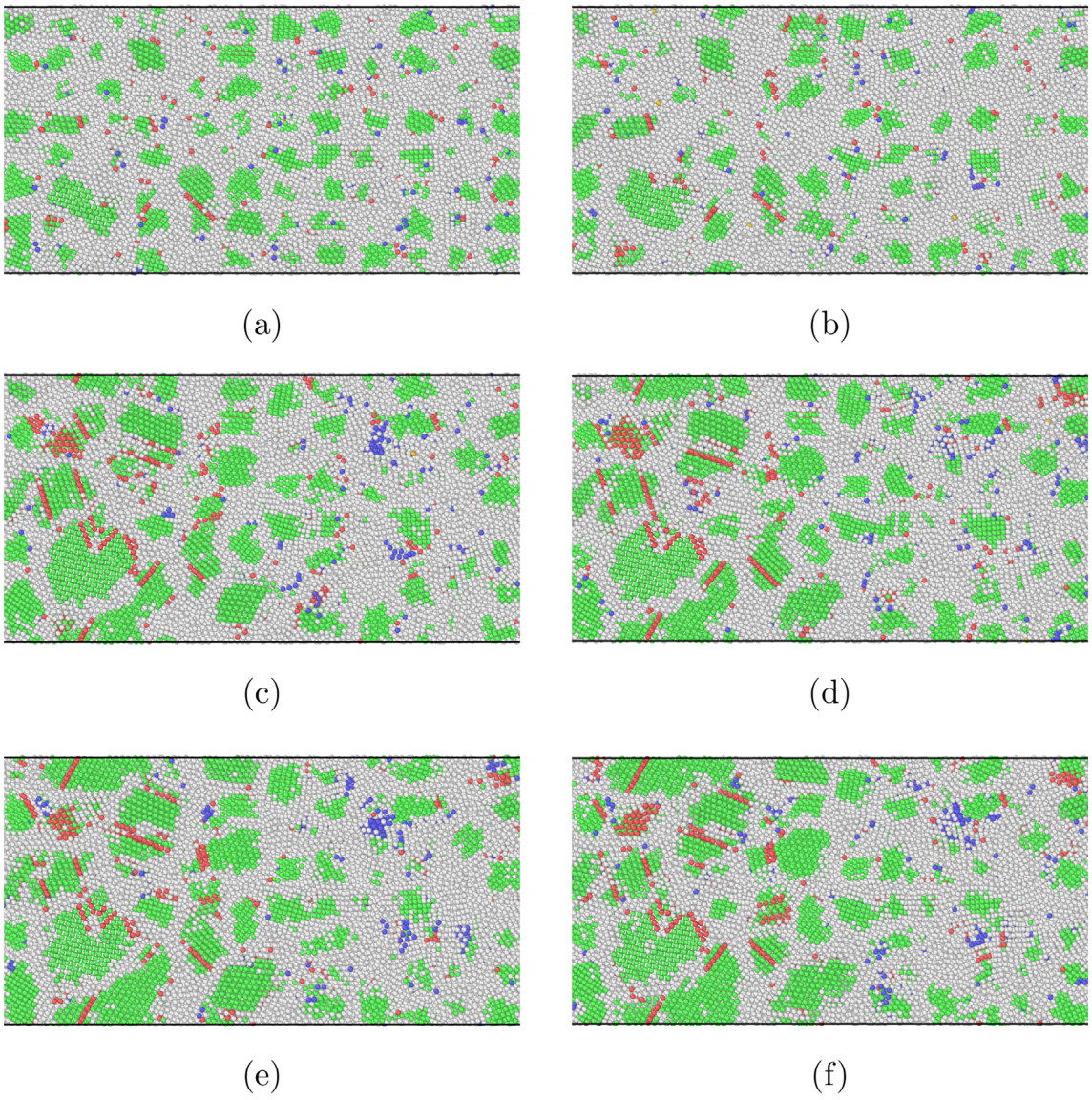

Fig. 4. The dislocation configuration simulated by MD in each microstate. The red and blue atoms represent the defect of dislocations and distortion. The green atoms represent prefect lattice structure and white atoms represent the grain boundary. (For interpretation of the references to colour in this figure legend, the reader is referred to the web version of this article.)

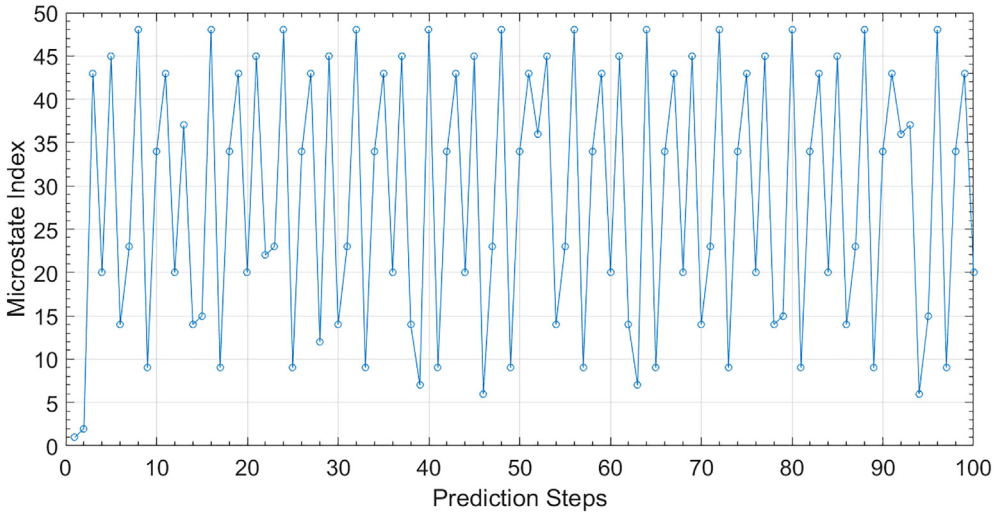

Fig. 5. The MSM result for the first 100 steps prediction. X is the MSM prediction step index, Y is the result of the microstate index shown in Table 5.

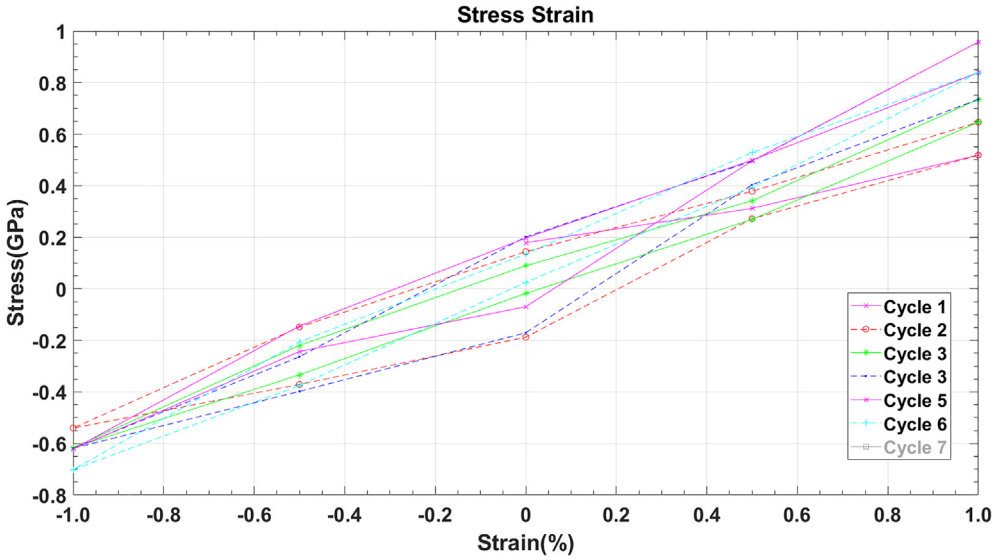

Fig. 6. The stress strain plot of MSM prediction.

term is the interatomic force potential contribution. The increase of broken bonds leads to the reduction of interatomic potential and following the atomic speed changes. Thus, a corresponding reduction of single atoms virial stress would be expected which induced the total system stress response to be reduced.

. Dislocation evolution

By investigating the associated atomic configuration Fig. 4, it was found that the dislocation formation presented in the first few cycles. The dislocation distributed in the γ phase more so than in the γ′ phase. Moreover, then the dislocation motion presents in the γ phase. The microstructure evolution of this MSM model results in a situation where energy minimisation favours the formation of new faults alongside existing ones. The following dislocation evolution will be discussed below.

. Dislocation formation and motion

Associated with the simulation result of the atomic model tessellation which is shown in Fig. 10, it is evident that the tendency of grain

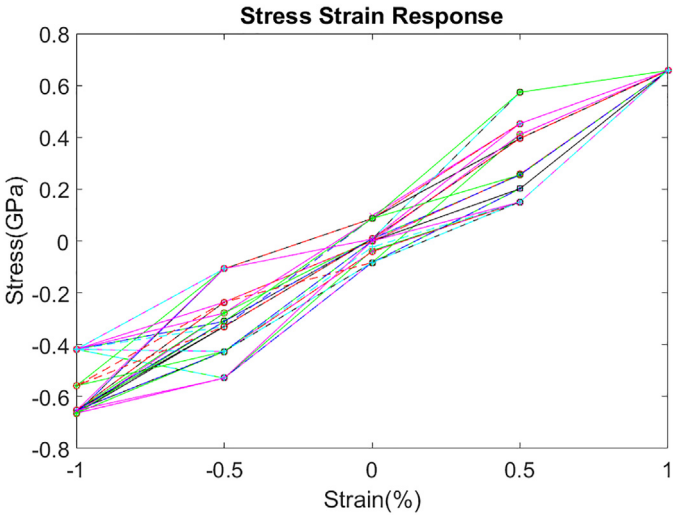

Fig. 8. A stress strain plot of MSM prediction with a vibration of valley stress.

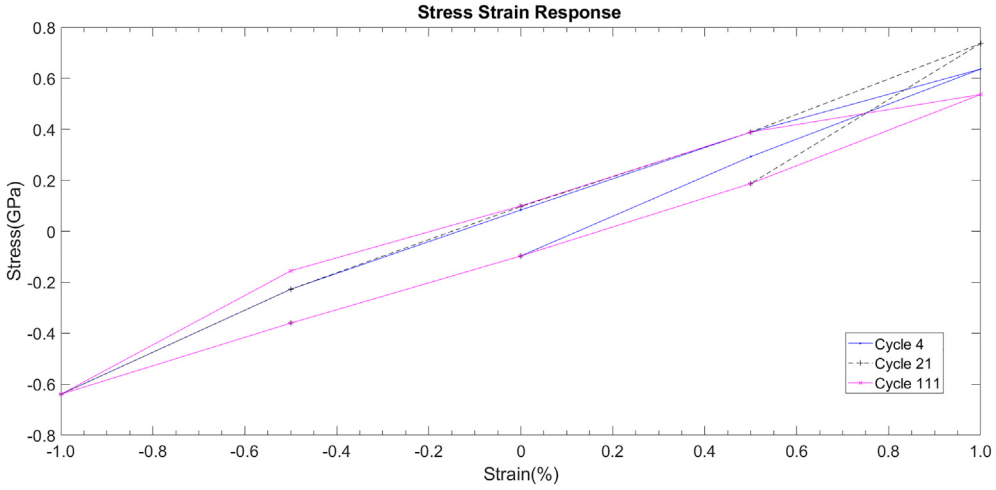

Fig. 7. The stress strain plot of MSM prediction for polycrystalline Nickel superalloy with strain amplitude 1.0% at temperature 873 K at cycle 4(Blue line), 21(Black line) and 111(Pink line). (For interpretation of the references to colour in this figure legend, the reader is referred to the web version of this article.)

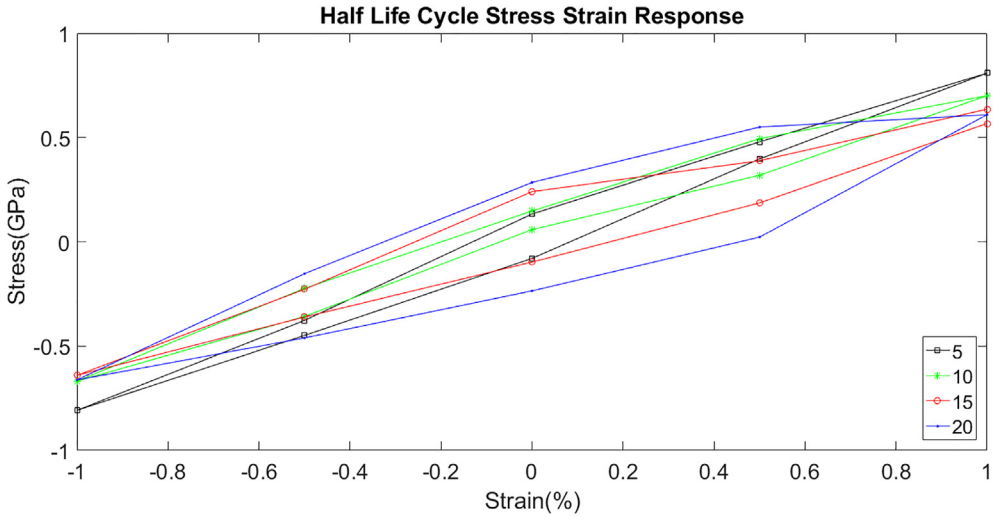

Fig. 9. The half life cycle stress strain response plot of MSM prediction for polycrystalline Nickel superalloy with strain amplitude 1.0% at temperature 873 K for test case with 5 Å, 10 Å, 15 Å and 20 Å broken bonds area in centre.

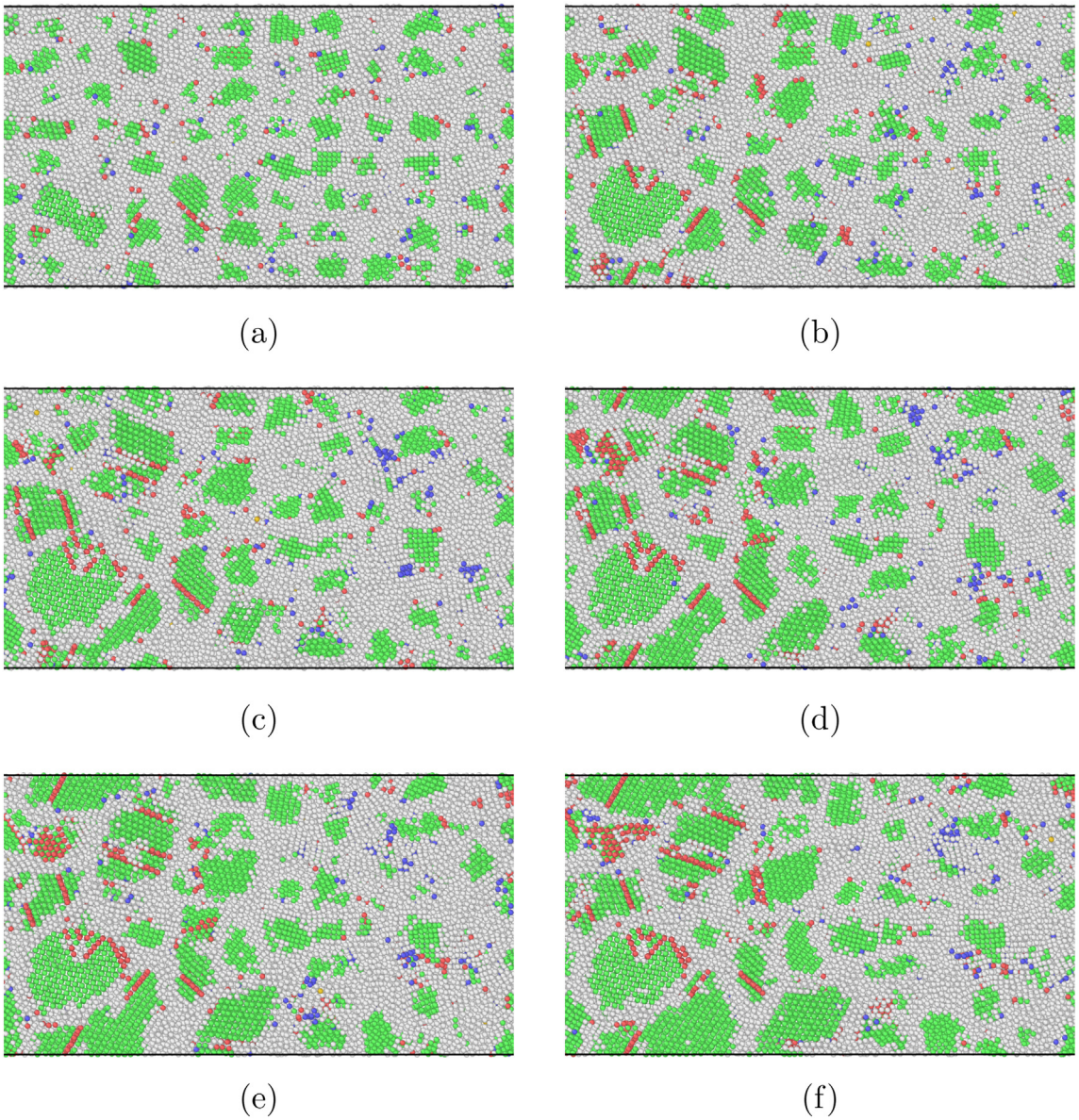

Fig. 10. Simulation result of the polycrystalline fatigue test with the dislocation formation and multiple cross-slip motion.

boundary dislocations accommodation could be observed in any situation. In the initial stage as shown in Fig. 10(a), it is almost dislocation free cause of the system start with a typical lattice configuration with enough relaxation at elevated temperature. After a few steps later at the 16th microstate as shown in Fig. 10(b), the grain boundary is much more identifiable than the first step and some dislocations accommodation are been observed near the grain boundary. After a few steps, the dislocations line grow due to the change of the simulation box which representing the deformation(Fig. 10(c)). After that, the dislocations reach steady-state and pile-up in the grain boundary as displayed in Fig. 10(d) to 10(f).

Another typical dislocation activity found in this situation is that some dislocations form and grow in the middle of a coarse grain as observed in Fig. 11. The dislocation formation according to the grain boundary evolution during cyclic loading. Because the grain angle of the two fine grains is high, the orientation of the atom changes easily under the external force. A strong agreement with the simulation result is that Masuda et al. [30] found that the grain protrusions or triple junctions are the original sites which transgranular dislocation activities start (Fig. 11(a)). From Fig. 11(b), a conspicuous dislocation could be found in the core of a new grain starting from a triple junctions grain boundary. After a few steps, a special cross slip of the dislocation starts with an angle to the main dislocation line (Fig. 11(d)). Associated with the repeated external load, the jog moves towards the grain boundary (Fig. 11(e) to 11(f)). Moreover, finally, a dislocation line is left in the middle of the new grain after the grain boundary disappeared and the transgranular dislocation accommodation across the core area of the γ phase side. Notably, the transgranular dislocations are parallel to each other in the core of grain along the close-packed plane which is a slip plane in FCC lattice.

. Grain boundary with dislocation

The grain boundary ledge which is an important source of dislocation during plastic deformation was also observed in Fig. 10(e). The dislocation could be emitted from the grain boundary by multiple cross-slip processes. The formation of the ledge remains by the dislocation motion through the grain boundary by external tension loading. The resulting boundary ledge can provide sites for dislocation nucleation under stress, for the reduction in boundary area at nucleation reduces the activation energy [31]. While in the γ' phase, the grain boundaries were not clear enough to be identified in most of the simulation results. However, when increasing the strain rate, the morphologies

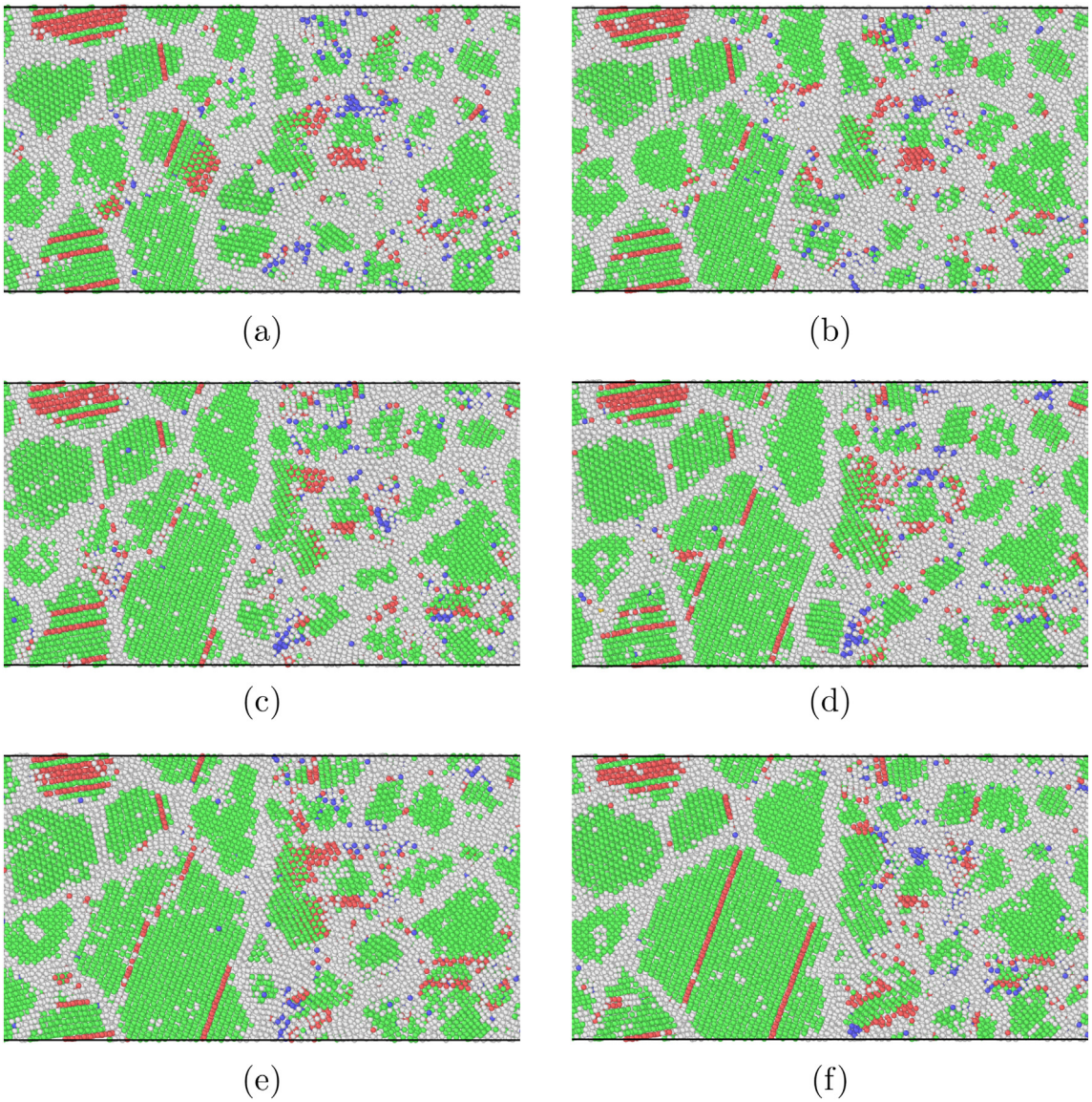

Fig. 11. Simulation result of the transgranular dislocation evolution.

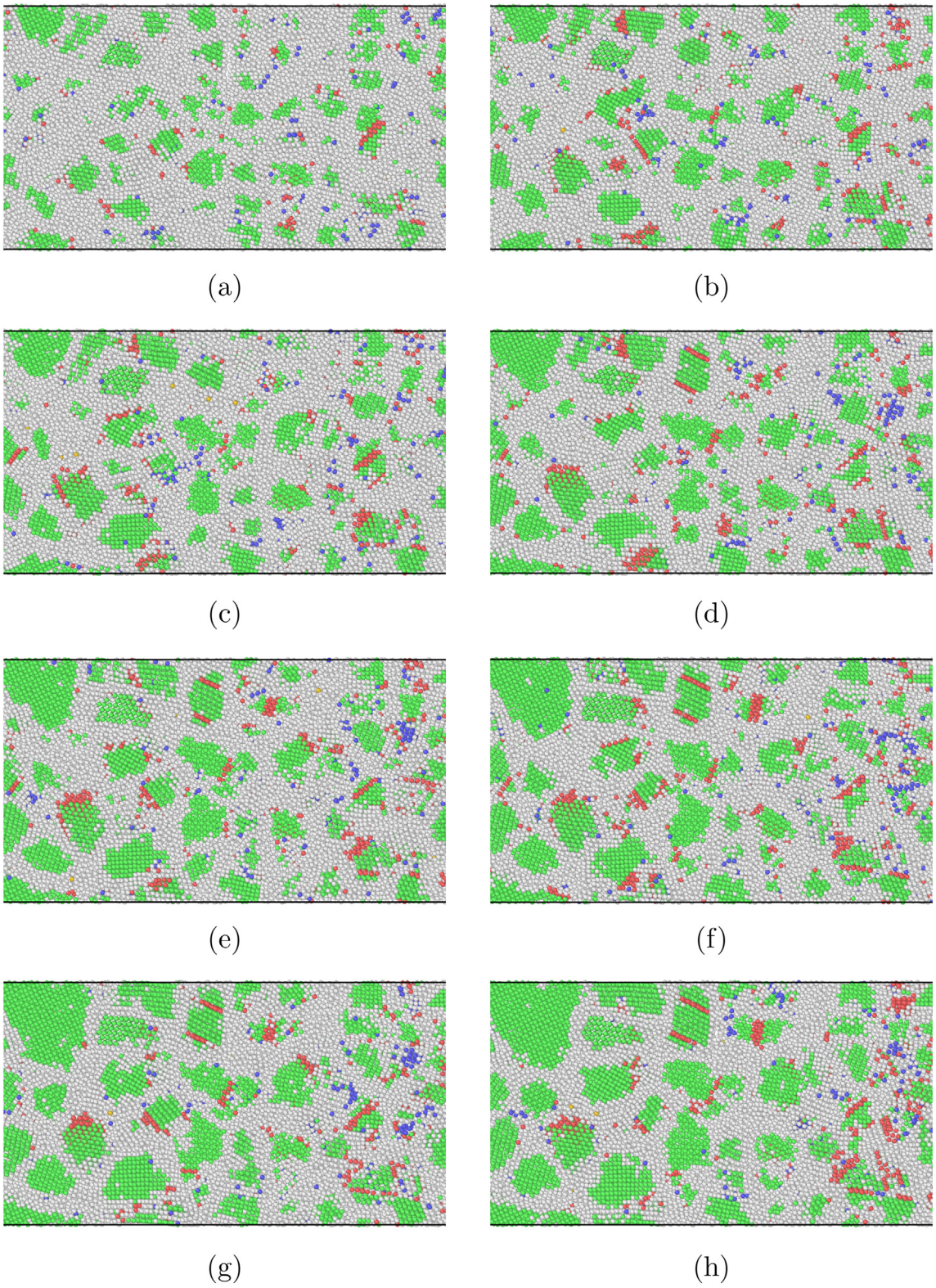

Fig. 12. Simulation result of the Polycrystalline Fatigue with dislocation accommodated in γ′ phase.

polycrystalline grain of the same model changes according to the boundary diffusion at elevated temperature from Fig. 13(b). Such a result was also reported in [32,33]. Also, the dislocations exhibit their activities in the γ′ phase which as displayed in Fig. 12. The dislocations first appear in the middle of the grain (Fig. 12(a)) then following dislocations dominated on the grain boundary (Fig. 12(b) - 12(h)) following by the cross-slip and climb. As discovered by [34,35], the dislocation motion in nickel superalloy γ′ precipitates phase produce misfit dislocation networks consistent with Lasalmonie and Strudel model which is a loss of coherency.

. Dislocation in γ and γ′ Phase

By examining all the test case tomography in OVITO, it found that dislocations occur are more active in grain or at the grain boundary in γ

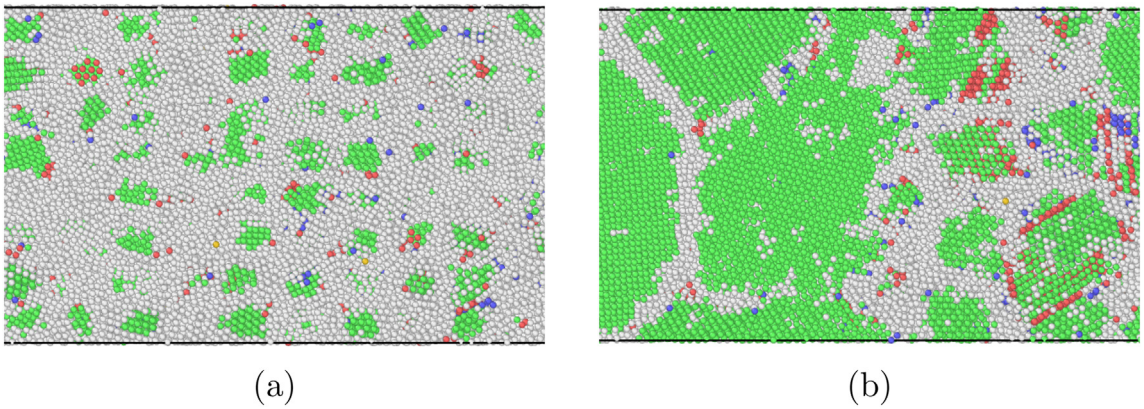

Fig. 13. Dislocations shows cross slip activities in γ′ phase at elevated temperature with a higher strain rate.

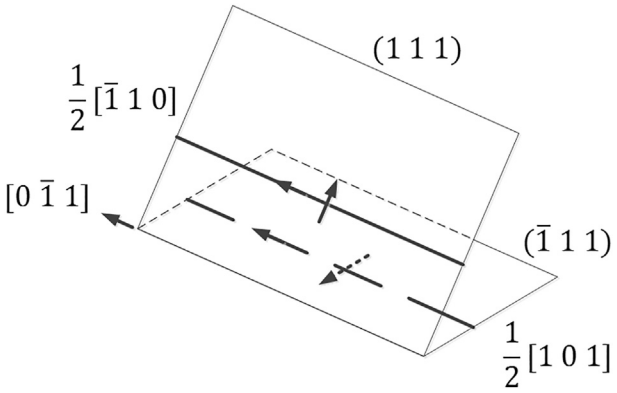

Fig. 14. Schematically illustration of Lomer dislocation. The two dislocations in {1 1 1} planes react to form a dislocation in the intersection line.

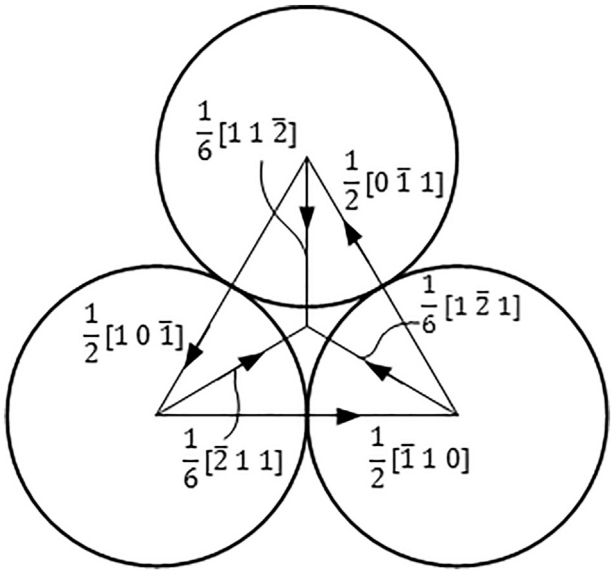

Fig. 15. Schematically illustration of perfect and Shockly dislocation in {1 1 1} planes.

phase than in γ′ phase. In γ phase, the dislocations are generated quickly in the first few stages, and then they are pile-up on the boundary or in the grain. The activity of the grain boundary and the atom inside come with the increased strain amplitude. However, in γ′ phase, once after the dislocations are formed, they steadily exist throughout the test no matter where they are accommodated. It indicates the interatomic bond of nickel and aluminium in FCC lattice are more stable than the pure interatomic bond of nickel atom in pure γ phase. In the γ′ phase, the grain boundary keeps its initial formation morphology as found in [36]. This indicates that γ′ phase is the stable strength phase in the nickel superalloy.

Another notable phenomenon in the result is that the length of dislocation line segments in γ phase is longer than that in γ′ phase. The expected dislocation on phase interface was also observed in our test cases because of the γ/γ′ interface overlay with the grain boundary. The parallel dislocation line can be noticed everywhere in the test case. These parallel dislocation lines decrease the motion ability of dislocation. Dislocations deposited on the γ/γ′ interfaces are in slip oriented segments. However, extensive cross slip results in an average line direction closer to those required for the most efficient accommodation of lattice mismatch.

. Hysteresis loop and energy dissipation

The hysteresis loop in the MD simulation indicates the plastic deformation according to the external loading. Since the MD simulation is strain-controlled, the total strain amplitude is always in the same value. However, the stress response could change due to the structure rearrangement. The result of the hysteresis loop is not clear from Fig. 6. This is due to the lack of sufficient checkpoints for microstate evolution. Also, another reason is the stress response in each microstate is measured by the atomic arrangement and their velocity which is affected by the temperature and ensemble configuration. But, by investigating into the detail of each cycle, the hysteresis loop could be clearly identified as displayed in Fig. 7. The result of hysteresis loop reveals a peak stress increase after a few cycles in the first stage and then decrease at the end of the test. From this image, it can be seen that the area of the hysteresis loop steadily increases. This indicates material hardening occurs at first and then the softening, while the plastic deformation constantly increases with the energy dissipation.

By comparing the stress-strain response result with other test cases which the broken bond area is increased, it seems the area of the hysteresis loop is proportional with this factor (Fig. 9). This configuration of the test model aims to simulate the situation of microcrack performed in the material due to the cyclical loading. The microcrack, a broken bond atomic configuration in this simulation, is an essential characteristic of fatigue loading [28]. In this result, the half-life cycle stress-strain responses of these test case with different size (5 Å to 20 Å) of microcrack were plotted in Fig. 9. The increase of the microcrack area, the higher hysteresis loop area are observed. This indicates that the energy dissipation increases associated with higher plastic deformation.

Also, when the microcrack size increased, the peak and valley stresses of fatigue response in this simulation are shrunk due to the extended broken bonds of atoms. This is relatively clear from Eq. 10. The increase of broken bonds leads to the reduction of interatomic potential and following the atomic speed changes. Thus, a corresponding reduction of single atoms virial stress would be expected which induced the total system stress response to be reduced.

. Dislocation evolution affects on fatigue

The dislocation motion is the elemental part of dislocation interaction. Since the dislocation systems are different in the different lattice structures, the dislocation interaction behaviour also has distinct characteristics accordingly. In FCC crystalline metal, the dislocation slip system is {111} <110>. The dislocation slip is a dynamic process by considering the stress state on the system. If the equilibrium of shear stress state on a unit cell was broken, the slip began. As known, if a moving dislocation is to bypass another one, the external stress is needed to overcome the maximum interaction force. Both the maximum interaction force and the necessary stress to overcome this force are proportional to the distance. During plastic deformation, the dislocation density increases and consequently the distance decreases. Thus, to continue plastic deformation, the applied stress has to increase.

The interaction behaviour between two dislocations depends on the dislocation types, the Burgers vector, the stress field of individual dislocation and their configuration. Generally, for two dislocations whose Burgers vectors parallel to each other, if their sign of Burgers vector is the same, and the combined stress field is more significant than that of a single dislocation, it leads to the energy of the configuration increasing and the dislocations will repulse each other. Thus, their interaction is dominated by their repulsive force.

If they have the opposite Burgers vector sign, the combined stress field is lower than that of the single dislocation, that will result in the compressive stress in this region from one dislocation overlapping with regions of tensile stress from the other dislocation. Finally, the attractive force will pull them close.

Actually, the dislocation Burgers vectors are not parallel in many situations, especially, for dislocations having cross slip planes which intersect each other. The Lomer dislocation [31] can be formed if two dislocation slips in their slip planes {111} which have a joint line $A1\beta = \left(1\ \underbrace{0\ 0\ \ldots\ 0}_{N-1}\right)^T$ as show in Fig. 14.

$$A1\beta = \left(1\ \underbrace{0\ 0\ \ldots\ 0}_{N-1}\right)^T \tag{11}$$

In most FCC lattices, each dislocation in close pack plane will be dissociated in its glide plane into two Shockley partial dislocations bounding a stacking-fault strip. If the dislocations crossover at the intersection line of the two slide planes, Frank's rule governs the interaction of the leading partials of the two dislocations. According to Frank's rule, their interaction could be repelled or attract depending on the configuration of Burgers vectors. Totally, there are 36 combinations to be considered during the interaction cause of the three possible $A1\beta = \left(1\ \underbrace{0\ 0\ \ldots\ 0}_{N-1}\right)^T$ slip vectors at both directions on each slip plane (Fig. 15). In these interactions, the most favourable reaction for plane (111) and $A1\beta = \left(1\ \underbrace{0\ 0\ \ldots\ 0}_{N-1}\right)^T$ which format a so-called stair-rod dislocation:

$$A1\beta = \left(1\ \underbrace{0\ 0\ \ldots\ 0}_{N-1}\right)^T \tag{12}$$

Notably, this kind of dislocation interaction results in the same total Burgers vector. According to Frank's rule, it will exert a repulsive force on the two Shockley partials and form a stable sessile arrangement which blocks further dislocation slips on the slip plane.

Moreover, the phenomenon of the grain boundary with great angle united according to the dislocation motion was also observed in this simulation. It is associated with lower stress of the system which could increase the ductility of the material but decrease the fatigue resistance.

. Conclusion

The MSM method integrated with MD simulation in nickel superalloy fatigue is a novel application which is based on the stochastic probability between a serial of Markov microstates of atomic superalloy models. The integrated MD microstates are predefined states which are based on the initialisation of the nickel superalloy atomic model and the dividable microstates for the whole fatigue cycle process. As known, the Markov state model has been applied in biomolecular dynamics for protein folding studies at the atomic scale to bridge the gap between macroscale and microscale [10,14]. The microstates of protein unfold process can be categorised as kinetic relevant microstates by the traditional MD clustering method such as k-means. However, this k-means method is not good for crystalline metal classification because the closed structure of the crystalline metal in the microscale is not like a protein atomic structure with notable features. But, in the atomic model of metal, the dislocation represented by the atomic arrangement is randomly distributed in the crystalline grain matrix. This type of atomic arrangement should have the typical dislocation structure similar to the protein molecular structure for proceeding with the categorisation process. However, the atomic dislocation structure could be emerged and evolved in a different location of the crystalline structure. Furthermore, the atomic arrangement with dislocation structures is difficult to define the *k* value in the k-means method. The selection of *k* is important for the result of k-means clustering which is not good for MSM initialisation state definition.

In this study, the MSM microstates were categorised according to the dislocation energy distribution criteria. This is based on the recognition of dislocation in the crystalline atomic model [27] which help the MSM microstates categorising with the dislocation energy classification according to the energy barrier theory [37]. This combined modelling approach has allowed probing at the atomic resolution of the dislocation evolution, which has remained challenging to accomplish by experiment. First, MD simulation samples were built up for the initialisation state of the MSM process. The dislocation motion and evolution among the metastable states where microstructure changes are essential during the fatigue process. The phenomenon of partial dislocation trend to dissociation was observed in this MSM simulation. This is a demonstration of the usefulness of the MSM approach in crystalline structure MD simulation. This finding agrees with the experiment but provides greater structural detail than experimental studies have so far been able to provide. Second, the phenomenon of the grain boundary with large angle united with the dislocation motion was also observed in this simulation. This dislocation motion along the grain boundary indicates the grain rotation and migration committed the grain boundary to fade among the high angle connection grains which have a strong agreement with experiment [30]. It is associated with lower stress of

the system which could increase the ductility of the material but decrease the fatigue resistance [30]. Also, the dislocation pile-up phenomenon was notable during the simulation. This activity was found on both grain boundary and phase boundary which increased the material APB energy which is associated with the enhanced strengthen.

The disadvantage of this MSM method on fatigue life prediction is that the limitation of the initialisation of microstates which have a profound influence on the result. Since the microstates are defined at the beginning of this MSM prediction process, the final result state must be one of the predefined microstates. However, in the reality of the real fatigue process, the final states of micro-crack initialisation and propagation could be dynamic with dislocation evolution. So, the result of this MSM methodology could be enhanced by revising the framework to a dynamic MSM method in future research work. By introducing the dynamics of the initial microstates in MSM, the initialisation is not fixed. Once the microstates evaluation after the MSM stage is finished, a new MD simulation process will be carried out based on the MSM result, and new MD simulation parameter also will be updated according to the MSM result. Once the MD process is finished, another circle of MSM stage begins. The new microstates will be classified, and the new probability matrix will be set according to the new energy barriers. The advantage of this new spiral up dynamic MSM method is that it would give a detailed result that is more accurate than that produced by the traditional MSM method. However, as it depends on the dynamics of the microstates and probability matrix redefinition thus make the process more complicated. Moreover, it would cost more on resource for MD computing and MSM matrix processing. This will increase the difficulty of the application of dynamics MSM method with MD simulation.

. Future works

In the near future, Our are planning to perform the following areas: (1) the virtual and physical verification and validation for the nickel superalloy fatigue analysis using digital twin technology; (2) high efficient design for the superalloy material using computational intelligence aided design (CIAD) [38]; (3) one step research towards AI-driven tools based on CIAD framework for material design.

Declaration of Competing Interest

None.

Acknowledgment

The authors would like to thank Glasgow Caledonian University, University of Strathclyde provide study and computing support for this research. Results were obtained using ARCHIE-WeST High Performance Computer (www.archie-west.ac.uk).

Data availability

The data used to support the findings of this study are available from the corresponding author upon request.

Declaration of Interest statement

The authors declare that they have no conflicts of interest.

Author contribution

Jianfeng Huang, Don McGlinchey and Yi Chen conceived the idea, Jianfeng Huang provided the theoretical analysis, Jianfeng Huang wrote a major portion of the manuscript, performed the numerical simulations and prepared all the figures. Daniel McMahon helped to publish the work. All authors reviewed the manuscript. The funders had no role in study design, data collection and analysis, decision to publish, or preparation of the manuscript.

References

[1] D.L. Logan, A First Course in the Finite Element Method, Cengage Learning 2011.
[2] W.-T. Ang, A beginner's Course in Boundary Element Methods, Universal-Publishers, 2007.
[3] C. Grossmann, H.-G. Roos, M. Stynes, Numerical treatment of partial differential equations, Vol. 154, Springer, 2007.
[4] G. E. Fasshauer, Meshfree approximation methods with MATLAB, Vol. 6, World Scientific, 2007.
[5] M. Fivel, Discrete dislocation dynamics: principles and recent applications, Multiscale Model. Heterogenous Mater. (2008) 17–36.
[6] F. Ercolessi, A Molecular Dynamics Primer, Spring College in Computational Physics, ICTP, Trieste 19 1997.
[7] S. Mesarovic, S. Forest, H. Zbib, Mesoscale Models from Micro-Physics to Macro-Interpretation, Springer, 2019.
[8] M.O. Steinhauser, Computational Multiscale Modeling of Fluids and Solids, Springer, 2017.
[9] W.-K. Ching, M.K. Ng, Markov Chains, Models, Algorithms and Applications, 2006.
[10] L.-T. Da, F.K. Sheong, D.-A. Silva, X. Huang, Application of markov state models to simulate long timescale dynamics of biological macromolecules, Protein Conformational Dynamics, Springer 2014, pp. 29–66.
[11] I. Horenko, E. Dittmer, F. Lankas, J. Maddocks, P. Metzner, C. Schütte, Macroscopic dynamics of complex metastable systems: theory, algorithms, and application to b-dna, SIAM J. Appl. Dyn. Syst. 7 (2) (2008) 532–560.
[12] M. Weber, A. Bujotzek, R. Haag, Quantifying the rebinding effect in multivalent chemical ligand-receptor systems, J. Chem. Phys. 137 (5) (2012), 054111, .
[13] M. Sarich, R. Banisch, C. Hartmann, C. Schütte, Markov state models for rare events in molecular dynamics, Entropy 16 (1) (2013) 258–286.
[14] G.R. Bowman, K.A. Beauchamp, G. Boxer, V.S. Pande, Progress and challenges in the automated construction of markov state models for full protein systems, J. Chem. Phys. 131 (12) (2009) 124101.
[15] V.S. Pande, K. Beauchamp, G.R. Bowman, Everything you wanted to know about markov state models but were afraid to ask, Methods 52 (1) (2010) 99–105.
[16] H. Hermanns, Markov chains, Interactive Markov Chains, Springer 2002, pp. 35–55.
[17] N. Singhal, V.S. Pande, Error analysis and efficient sampling in markovian state models for molecular dynamics, J. Chem. Phys. 123 (20) (2005) 204909.
[18] K.M. Thayer, B. Lakhani, D.L. Beveridge, Molecular dynamics–markov state model of protein ligand binding and allostery in crib-pdz: conformational selection and induced fit, J. Phys. Chem. B 121 (22) (2017) 5509–5514.
[19] R. Metzler, J. Klafter, From a generalized chapman- kolmogorov equation to the fractional klein- kramers equation, J. Phys. Chem. B 104 (16) (2000) 3851–3857.
[20] E. Rosta, G. Hummer, Free energies from dynamic weighted histogram analysis using unbiased markov state model, J. Chem. Theory Comput. 11 (1) (2014) 276–285.
[21] V.A. Voelz, G.R. Bowman, K. Beauchamp, V.S. Pande, Molecular simulation of ab initio protein folding for a millisecond folder ntl9 (1- 39), J. Am. Chem. Soc. 132 (5) (2010) 1526–1528.
[22] F. NoÃ©, E. Rosta, Markov models of molecular kinetics, J. Chem. Phys. 151 (19) (2019) 190401 , arXiv https://doi.org/10.1063/1.5134029.
[23] G.V. Cormack, R.N.S. Horspool, Data compression using dynamic markov modelling, Comput. J. 30 (6) (1987) 541–550.
[24] J.-F. Huang, Z.-L. Wang, E.-F. Yang, D. McGlinchey, Y.-X. Luo, Y. Li, Y. Chen, Molecular dynamics simulation of persistent slip bands formation in nickel-base superalloys, Int. J. Autom. Comput. 14 (1) (2017) 68–79, https://doi.org/10.1007/s11633-016-1035-x.
[25] Y. Mishin, Interatomic Potentials for Metals, Springer, 2005.
[26] F. Fritzen, T. Böhlke, E. Schnack, Periodic three-dimensional mesh generation for crystalline aggregates based on voronoi tessellations, Comput. Mech. 43 (5) (2009) 701–713.
[27] J. Huang, D. McGlinchey, Y. Luo, Y. Chen, A computational intelligence based dislocation recognition during molecular dynamics simulation, Automation and Computing (ICAC), 2016 22nd International Conference on, IEEE 2016, pp. 225–232.
[28] W.-P. Wu, Z.-Z. Yao, Molecular dynamics simulation of stress distribution and microstructure evolution ahead of a growing crack in single crystal nickel, Theo. Appl. Fract. Mech. 62 (Supplement C) (2012) 67–75, https://doi.org/10.1016/j.tafmec.2013.01.008http://www.sciencedirect.com/science/article/pii/S0167844213000098.
[29] M.J. Buehler, Atomistic Modeling of Materials Failure, Springer Science & Business Media, 2008.
[30] H. Masuda, H. Tobe, E. Sato, Y. Sugino, S. Ukai, Transgranular dislocation activities and substructural evolutions accommodating two-dimensional grain boundary sliding in ods ferritic steel, Acta Mater. 132 (2017) 245–254.
[31] D. Hull, D.J. Bacon, Introduction to Dislocations, Butterworth-Heinemann, 2001.
[32] H. Zhang, S. Zhang, M. Cheng, Z. Zhao, Microstructure evolution of in718 alloy during the delta process, Proc. Eng. 207 (2017) 1099–1104.
[33] D. Bridges, R. Xu, A. Hu, Microstructure and mechanical properties of ni nanoparticle-bonded inconel 718, Mater. Des. 174 (2019) 107784, https://doi.org/10.1016/j.matdes.2019.107784http://www.sciencedirect.com/science/article/pii/S0264127519302217.
[34] A. Singh, N. Louat, K. Sadananda, Dislocation network formation and coherency loss around gamma-prime precipitates in a nickel-base superalloy, Metall. Trans. A. 19 (12) (1988) 2965–2973.

[35] N.-L. Li, W.-P. Wu, K. Nie, Molecular dynamics study on the evolution of interfacial dislocation network and mechanical properties of ni-based single crystal superalloys, Phys. Lett. A 382 (20) (2018) 1361–1367, https://doi.org/10.1016/j.physleta.2018.03.031http://www.sciencedirect.com/science/article/pii/S0375960118302901.

[36] W.-S. Ko, S.B. Maisel, B. Grabowski, J.B. Jeon, J. Neugebauer, Atomic scale processes of phase transformations in nanocrystalline niti shape-memory alloys, Acta Materialia 123 (2017) 90–101, https://doi.org/10.1016/j.actamat.2016.10.019 , URL http://www.sciencedirect.com/science/article/pii/S1359645416307832.

[37] S. Aubry, K. Kang, S. Ryu, W. Cai, Energy barrier for homogeneous dislocation nucleation: comparing atomistic and continuum models, Scr. Mater. 64 (11) (2011) 1043–1046.

[38] Y. Chen, Y. Li, Computational Intelligence Assisted Design (In the Era of Industry 4.0), CRC Press, 2018.